CASL-U-2015-0020-000

Improvement of COBRA-TF Subchannel Thermal-Hydraulics Code (CTF) using Computational Fluid Dynamics

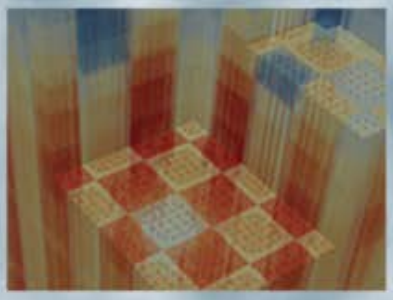

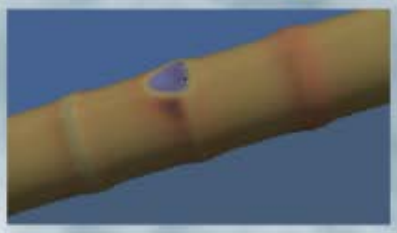

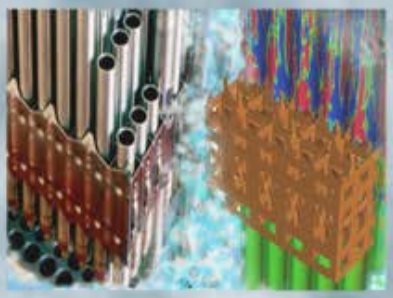

Taylor S. Blyth
Pennsylvania State University

December 15, 2014

CASL-U-2015-0020-000

Improvement of COBRA-TF Subchannel Thermal-Hydraulics Code (CTF) using Computational Fluid Dynamics

Taylor Blyth, The Pennsylvania State University, tyb5095@psu.edu 15 December 2014

Abstract

This report presents a proposal for improving the CTF subchannel thermal hydraulics code using computational fluid dynamics data. CTF modeling capabilities can be improved by capturing the following four phenomena: (1) grid directed lateral cross-flow effects, (2) grid-induced turbulent-mixing effects, (3) grid-induced heat transfer enhancement downstream of the grid, and (4) the detailed pressure-loss effects caused by the spacer grid. The first two effects have already been captured with work done by Avramova (2007) [1] and have been implemented into the current version of CTF; however, more work may be needed to make these features accessible and more useful for CTF users. A proposal is presented in this document for how phenomena 3 and 4 will be captured.

CTF Conservation Equations

The following proposed improvements will involve modifications to the CTF governing equations. Within CTF there are three main conservation equations that are solved for each phase—mass, momentum, and energy. For each of the following conservation equations, the subscript k is used to denote the phase—either vapor (v), liquid (l), or entrained droplet (e).

General Phasic Momentum Conservation Equation

$$\frac{\partial}{\partial t}\left(\alpha_k \rho_k \vec{V}_k\right) + \frac{\partial}{\partial x}\left(\alpha_k \rho_k u_k \vec{V}_k\right) + \frac{\partial}{\partial y}\left(\alpha_k \rho_k v_k \vec{V}_k\right) + \frac{\partial}{\partial z}\left(\alpha_k \rho_k w_k \vec{V}_k\right) = \alpha_k \rho_k \vec{g} - \alpha_k \nabla P + \nabla \cdot \left(\alpha_k \tau_k^{ij}\right) + \vec{M}_k^L + \vec{M}_k^d + \vec{M}_k^T \tag{1}$$

On the LHS of this equation:

- The first term is the change in volume momentum over time
- The next three terms account for advection of momentum in each of three directions

On the RHS of this equation:

- The first term is the gravitational force
- Second is the pressure force
- Third is the viscous shear stress, which captures wall drag and form losses
- Fourth is the momentum source term due to phase change and entrainment/de-entrainment
- Fifth is the interfacial drag source term
- Sixth is the momentum source term due to turbulent mixing and void drift

General Phasic Energy Conservation Equation

$$\frac{\partial}{\partial t}\left(\alpha_k \rho_k h_k\right) + \nabla \cdot \left(\alpha_k \rho_k h_k \vec{V}_k\right) = -\nabla \cdot \left(\alpha_k \vec{q}_k^T\right) + \Gamma_k h_k^i + q_{wk}''' + \alpha_k \frac{\partial P}{\partial t} \tag{2}$$

On the LHS of this equation:

- The first term is the change of energy over time
- Second is the advection of energy

On the RHS of this equation:

- The first term is the inter-cell energy exchange due to void drift and turbulent mixing

CASL-U-2015-0020-000

- Second is the energy transfer due to phase change
- Third is the volumetric wall heat transfer
- Fourth is the work done on the fluid cell due to pressure

General Phasic Mass Conservation Equation

$$\frac{\partial}{\partial t}(\alpha_k \rho_k) + \nabla \cdot \left(\alpha_k \rho_k \vec{V}_k\right) = L_k + M_k^T \tag{3}$$

On the LHS of this equation:

- The first term is the change in mass over time
- The second is the advection of mass

On the RHS of this equation:

- The first term is the mass transfer into or out of phase k (e.g. evaporation/condensation)
- The second is the mass transfer due to turbulent mixing and void drift

The CTF theory manual [2] covers the conversion of these general phasic conservation equations to a discretized form that can be solved numerically for the independent variables of the current iteration: phase enthalpy, phase mass, mixture pressure, and phase velocity.

Grid-Directed Cross-Flow Model

M. Avramova's 2007 thesis [1] discusses the changes made to CTF in order to allow for external, CFD-produced data tables to be used during calculations involving spacer grids. The directed crossflow model accounts for the lateral flow caused by the mixing vanes on grids. This option gives the user the ability to use data from a specific spacer grid and apply it to a subchannel calculation, allowing for the capture of the basic effect of the grid on lateral flow with reduced computation expense in comparison to CFD.

This model adds an additional source term to the liquid lateral momentum equation that captures the grid-directed cross-flow effects. The modified subchannel form of the liquid transverse momentum equation is shown below.

$$\begin{aligned}&\frac{\partial}{\partial t}\left(\alpha_l \rho_l \vec{V}_l\right) + \frac{\partial}{\partial x}(\alpha_l \rho_l u_l v_l) + \frac{\partial}{\partial y}(\alpha_l \rho_l v_l v_l)\\ &= \alpha_l \rho_l \vec{g} - \alpha_l \nabla P + \nabla \cdot \left(\alpha_l \tau_l^{ij}\right) + \vec{M}_l^L + \vec{M}_l^d + \vec{M}_l^T + \vec{M}_l^{GDCF}\end{aligned} \tag{4}$$

The final term in the equation, $\vec{M}_l^{GDCF}$, is the source term representing grid-directed cross-flow effects. The derivation of this factor is based on the results from the CFD simulation of a similar geometry model. The definition of this source term is shown in Equation (5).

$$\vec{M}_l^{GDCF} = {f_{lat,SG}}^2 \left(u_l^2\right)(\rho_l) A_{gap} \mathrm{S} \tag{5}$$

where:

- $f_{lat,SG}$ is the lateral convection factor
- u_l is the axial liquid velocity
- ρ_l is the liquid density
- A_{gap} is the cross-sectional area of the gap
- S is a factor to account for the direction of the force (either -1, 0, or 1)

Most of these terms will be supplied by CTF—the lateral convection factor, $f_{lat,SG}$, and direction factor, S, must be supplied by external input file (please see Appendix A and Appendix B for examples of the external input file form). The lateral convection factor should be calculated by means of a CFD simulation. It is defined as the ratio between lateral and inlet axial velocity at a given location downstream of the grid [3]:

$$f_{lat,SG}(z - z_g) = \frac{V_{z-z_g}^{CFD}}{U_{inlet}^{CFD}} \tag{6}$$

where:

- $z - z_g$ is the downstream distance from the spacer grid

These factors will be supplied at many axial locations as a table in the external input file and they will be specific to the geometry modeled by the CFD simulation.

The direction factor must be supplied for each gap in the model. Currently, this file must be manually created by the user with consideration for the vane directions of the mixing vane grids. The values for each gap are either -1, 1, or 0. A zero means that the factor will not be applied at that gap. The positive/negative signs indicate whether it is flow from a lower-to-higher numbered subchannel or vice versa. Figure 1 is a visual representation of the data that are included in the mapping file. In this figure, only the gaps of internal-internal subchannel connections are assumed to have any crossflow. This is because the CFD data from which these factors were taken did not simulate any other type of connection such as corner-side or side-side. The pattern of the flow can still be seen which is caused by the orientation of the mixing vanes on the grid. Appendix B contains the actual contents of the mapping file for reference.

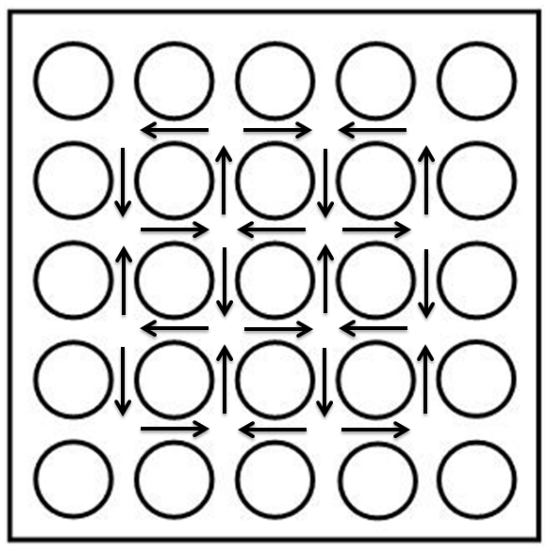

Figure 1: Sample 5x5 geometry for the mapping file

Grid-Induced Turbulent-Mixing Model

The turbulent mixing model accounts for a specific grid geometry's effect on the two-phase mixing multiplier. This model allows the user to supply a multiplicative factor for the two-phase phase component of turbulent mixing. These correspond to term $\vec{M}_k^T$ in Equation (1), Term $\nabla \cdot \left(\alpha_k \vec{q}_k^T\right)$ in Equation (2), and Term M_k^T in Equation (3). This factor, f_θ, is applied to the two-phase portion of the mixing source terms only. These are defined in CTF for transverse mass flow caused by turbulent mixing as follows:

$$W_{ij}^M = \frac{\beta_{\mathrm{tp}} \bar{G}}{\bar{\rho}_{mix}} \left(G_{iz} - G_{jz}\right) A_{gap} \tag{7}$$

where:

- W_{ij}^M is the lateral mixing of mass due to turbulence
- β_{tp} is the two-phase mixing coefficient
- $\bar{G}$ is the average axial mass flux between subchannels i and j
- ρ_{mix} is the average mixture density between subchannels i and j
- G_{iz} and G_{jz} are the axial mass fluxes of subchannels i and j, respectively
- A_{gap} is the cross-sectional area of the gap

Mixing of energy and momentum are similarly defined and can be found in the CTF Theory Manual [2].
The grid-induced turbulent-mixing model is applied by modifying the mixing coefficient, β_{tp}, using a factor, f_θ.

$$\beta_{tp}=\beta_{tp}f_\theta \tag{8}$$

Similar to the grid-directed cross-flow model, f_θ is calculated from a CFD simulation of the geometry of interest and should be supplied by an external file to CTF. The $f_\theta$factor is defined as follows:

$$f_\theta(y,\varphi)=\frac{\beta_{SP}^{spacers}}{\beta_{SP}^{no\ spacers}} \tag{9}$$

The factor is a function of the distance downstream of the grid, y, and the vane angle, φ. The single-phase mixing coefficient values were determined using CFD parameters, as the mixing coefficient is not a value directly available from CFD results. There are three main methods used to calculate the value: using the surface-averaged values, using the gap-averaged values, and using a local heat balance. This factor peaks at the upper edge of the mixing vanes and then decreases until the flow reaches the next grid. And, as expected, if the vane angle of the grid increases then the ratio will increase as well.

The f_θ values in the CFD data file (please see Appendix C for an example) come from multiple parameters. Since the factor is applied to each subchannel at each axial location, no mapping file is required as was for the directed crossflow portion. The data extracted from the CFD simulations used in the creation of these factors include:

- The volume-averaged fluid density of subchannel i
- The volume-averaged axial velocity of subchannel i
- The volume-averaged specific heat of subchannel i
- The surface-averaged fluid temperature at the inlet and outlet of subchannel i
- The average volume-averaged specific heat over subchannels i and j
- The average volume-averaged fluid densities over subchannels i and j
- The average volume-averaged axial velocity over subchannels i and j
- The volume-averaged fluid temperature of subchannels i and j

Setting up the surface and volume averaging across the subchannels is important for this step. A diagram of the geometry is shown in Figure 2. There are two adjacent subchannels, i and j, which have different inlet temperatures. They are broken down axially and at each axial node a value for the β_{tp} multiplier is reported.

Volume-averaging is done over the entire cell's fluid domain defined by the subchannel's lateral and axial boundaries. The surface-averaging is performed over the entire lower or upper surface of the cell. The f_θ factor from Equation (9), a ratio of the β_{SP} mixing coefficients, is defined using a heat balance method:

$$\beta_{SP}=\frac{\rho_i U_i A_i^{flow} c_p\left(T_i^{out}-T_i^{in}\right)}{S_{ij}\,\Delta x\overline{c_p}\overline{\rho}\overline{U}\left(T_j-T_i\right)} \tag{10}$$

Here, the S_{ij} term is the gap width and Δx is the axial height of the cell.

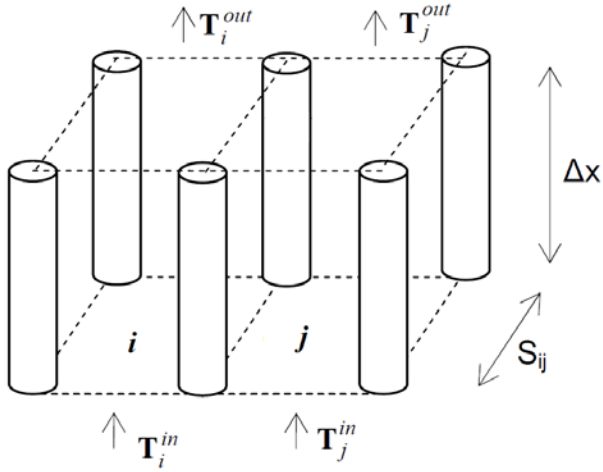

Figure 2: 2x1 subchannel layout used for the CFD determination of the mixing coefficient factor [1]

Summary and Comments on the Previously-Developed Models

These options give the users a good opportunity to improve the accuracy of their models by allowing for specific grid geometry data, but there are a few deficiencies as well. For the directed crossflow, the user must apply the same factor across each gap where the model is applied. There is currently no ability to account for the different types of subchannel gap connections, such as corner-side, side-side, or side-internal. One way to solve this could be to add another map of the geometry and specify more detailed factors that can be applied to the main lateral convection factor. These detailed factors must come from the CFD data as well, and would require a full-size simulation.

It would also be preferable if the mapping file could be generated in an automated way, perhaps using the CTF preprocessor. Currently, utilizing these models involves a great deal of manual intervention. Also, realistic PWR simulations are going to be different than most experimental results (which would likely contain shrouds that create corner and side subchannels where a real PWR will have no bounds on its side/corner subchannels) and therefore the predicted results are going to be different than most experimental cases, such as the PSBT results. In an actual core, crossflow may come from other assemblies as well as the inter-assembly vane angle effects, and this will be difficult to completely capture in a simple model. This type of model also does not allow the user to specify different types of grids along the axial domain. All grids that are to have these effects modelled will have the same lateral convection and turbulent mixing factors.

Proposed CFD-Informed Heat-Transfer Model

Altering the geometry of the flow area by means of introducing grids causes differences in the flow around the grid. A spacer grid impacts the downstream heat transfer by the following means:

- Boundary layer disruption due to additional surfaces—both the hydrodynamic/velocity BL and the thermal BL
- Skin friction along the grids which alters the local axial and lateral velocities
- Thermal radiation from the rod surface to the grid through the fluid (only significant at very high temperatures)
- Fin cooling effect of the rod surface being in contact with the spacer grid, which is then exposed to the flow
- Just upstream of the grid the flow is accelerated and this causes a difference in rod surface temperatures
- Diversion of the flow around the non-negligible grid strap thickness as the flow contacts the leading edge

As fluid passes over a surface, its surface friction causes a boundary layer to form along the length of the surface in the direction of the flow. This is a layer where the fluid moves slower than the free-stream velocity and therefore cannot convect as much heat from the surface. Its presence acts to shield the surface from the direct effects of the bulk fluid. The thickness of this boundary layer varies with the distance downstream of its initial formation. At the point of onset, there is no boundary layer. If flow conditions remain constant, the boundary layer will grow downstream of this initial point. The thickness profile decreases with increasing Reynolds number—whether due to an increase in velocity or a decrease in viscosity. For turbulent flow such as that in an LWR, the boundary layers are not as thick or discrete as they would be in laminar flow. This means that as the Reynolds number increases, the boundary layer has less of a diminishing effect on the rod-to-fluid heat transfer. As expected, disruption of the boundary layer would improve the heat transfer from the surface to the fluid. The points where the rod is in contact with the spacer grid will stem a boundary layer disruption.

These are the springs/dimples, and there are usually four of them in contact equally spaced around the rod—even on the simple spacer grid geometries. A larger rod pitch will decrease the overall effects from boundary layer formation due to the fact that the boundary layer's dimension will become smaller in comparison to the distance between the rod's surface and the grid's strap.

With additional surface area within the subchannel there will be increased viscous drag force acting on the flow. The presence of grids also decreases the flow area due to non-negligible strap thickness. This causes local acceleration of the flow through the decreased area and this effect is present just upstream of the grid as well. Impingement upon the leading edges of the grid is dependent on the profile of the leading edge (roundness and thickness) and will cause some diversion of the flow from its original path. This results in small lateral velocities at the location of the grid. Where there is contact between the rod surface and the grid, there is a fin cooling effect due to the conduction of heat from the rod surface to the cooler spacer grid material which acts as a heat sink dispersing energy into the passing fluid. This cooling would cool the area on the rod surface where the grid dimple is in contact, causing local temperature differences azimuthally around the rod. This is not a very strong effect however, as there is little contact area and the temperature difference between the bulk fluid and the rod surface is not significant enough.

Not all of these heat transfer modifications apply to each type of grid found in an LWR. The means of accounting for these effects are broken down for each of the three main types of spacer grids: egg-crate (simple) spacers, mixing-vane (crossflow) grids, and split-vane (swirl) grids.

Effects of each grid type:
Egg-crate type grids are used in bundles to keep the rods in their correct positions while allowing for thermal expansion and limited movement. They are constructed of thin metal plates (straps) which are about 0.5 mm thick and generally around 10 – 50 mm long. These simple spacers hold the rods in position with springs, which are dimple cut-outs that protrude from the metal strap itself and meet the rod at its expected position. Usually there are four such cut-outs in order to confine the rod from all four sides (top, bottom, left, and right as viewed from above). These spacers directly cause minimal boundary layer disruption as the flow is not diverted onto the rods and there is not much grid material within the rod's boundary layer. The main effect of the egg-crate spacers is likely the change in axial velocity caused by the contraction and expansion of the flow due to geometry. Since these velocity changes occur within the length of the grid, CTF is not able to properly capture their effects as the grids can exist in a single fluid mesh cell. As the flow enters then exits the reduced flow area of the grid it may slightly disrupt the rod surface's boundary layer. This is due to the fact that more fluid will be closer to the surface and therefore it will allow for more heat to be removed if the turbulent boundary layer is even slightly altered.

Split-vane grids are used in bundles to create intra-channel swirl in order to augment the downstream heat transfer within a subchannel. These cause vortices within each subchannel and impose minimal crossflow across the gaps. The swirl created by these grids both disrupts the boundary layers on the rod surfaces and creates additional lateral flow. It is proposed to have CTF account for these swirling-vane grids by having an increased lateral velocity term in the calculation of its local Reynolds number. The augmented Reynolds number is then used to obtain a HTC from the Dittus-Boelter correlation. In this manner, the actual velocities inside the mesh cell are not altered. The procedure for applying a swirl factor is described in more detail later in this section.

Mixing-vane grids are used to create cross-flow between subchannels. The vanes on these grids are similar to those of the split-vane grids, but angle the flow in a meandering pattern instead of a circular pattern. This type of flow creates a different effect at each of the rod surfaces within a subchannel. Therefore, the same swirl factor cannot be applied at each of the surfaces in order to calculate an updated HTC. The HTC will differ for each surface due to the local flow caused by the grid. There may even be stagnation points present within the subchannel in the 2-D axial plane which could increase the likelihood of DNB onset. Flow reduction transients would augment the chances for the establishment of DNB if there were a stagnation point in the lateral flow, but normal scenarios would not face this issue—the axial flow will remain almost the same as the bulk fluid velocity and this should keep DNB from occurring. With the meandering flow pattern, approximately half of the rods surfaces will experience a large increase in lateral velocity while the other half will experience negligible lateral velocities. The proposed method for CTF to account for these grid-specific differences based on CFD measurements is to utilize a data file in order to give the code the rod surfaces over which the lateral flow is increased. This will hold data for all of the rod surfaces contained by the fluid subchannels. Then, within this file, there will be a factor associated with each of these surfaces. The factor will be a lateral velocity factor, and can be captured in the same method as it is for the swirl-inducing vanes.

Consider how the Yao/Hochreiter/Leech (YHL) model is currently used within CTF to predict the change in heat transfer. The YHL formula is used to calculate an enhanced heat transfer due to the effect of a grid, which is applied to the CTF energy equation similarly to the implementation in above. The YHL correlation is a function of the projected area of the grid, the vane angle, and the distance downstream of the grid. The correlation was developed from experimental data involving a collection of different grid types used in varying operating conditions. The correlation augments the dimensionless Nusselt number, which can be calculated by CTF. This allows for the application of the heat transfer enhancement model in a variety of different conditions. The original correlation, as it appears as a multiplier in CTF, is:

$$\frac{Nu}{Nu_0} = \left[1 + 5.55\epsilon^2 \exp\left[\text{-}0.13\frac{x}{D}\right]\right]\left[1 + A^2 \tan^2(\Phi) \exp\left[\text{-}0.34\frac{x}{D}\right]\right]^{0.4} \tag{11}$$

Here, Nu is the Nusselt number (the subscript 0 refers to the bare grid geometry), ϵ is the blockage ratio, $\frac{x}{D}$ is the dimensionless distance downstream from the grid, A is the projected area of the grid, and Φ is the vane angle with respect to the flow. The coefficients in this equation can be altered by the user, allowing them to turn off the mixing vane portion of the correlation. This correlation results in heat transfer enhancement being largest at the grid exit and decaying exponentially as downstream distance from the grid increases. CTF input allows users to tune the parameters of Equation (11) by specifying coefficients as well as the blockage ratio and the vane angle.

The Reynolds number is used to calculate the heat transfer coefficients (HTCs) of various flow regimes within CTF. The single-phase liquid regime, for instance, then calculates its heat transfer coefficient for rod-to-fluid convection based either on this calculated HTC or by using a constant value, depending on which is greater. This is shown in Equation (12). Fluid velocity affects the Reynolds number, and therefore it needs to be corrected if a grid is going to cause local changes in velocities. The Nusselt number is used in CTF in order to calculate the HTCs.

$$Nu = \frac{hL}{k} \tag{12}$$

The HTC for a surface in the subchannel is defined as the heat flux over the difference in wall and bulk fluid temperatures as shown in Equation (13).

$$h = \frac{q''}{\Delta T} = \frac{q''}{T_{wall} - T_{bulk}} \tag{13}$$

The HTC is extracted from the Nusselt number, such as the Dittus-Boelter correlation, by solving Equation (12) for the h value. This explains the appearance of the k (thermal conductivity) and D (hydraulic diameter) terms in Equation (14).

$$h_{spl} = \max\begin{cases} 0.023\frac{k_l}{D_h}Re^{0.8}Pr^{0.4} \\ 7.86\frac{k_l}{D_h} \end{cases} \tag{14}$$

Equation (14), for the single-phase liquid heat transfer coefficient, contains the Reynolds number as well as the Prandtl number. The Reynolds number is stated in Equation (15) in terms of the subchannel parameters.

$$Re = \frac{\rho U D}{\mu} \tag{15}$$

Here, ρ is the fluid density, μ is the dynamic viscosity, U is the fluid velocity, and D is the equivalent (hydraulic) diameter of the fluid volume cell. Currently within CTF, the subchannel's axial velocity and its lateral velocity are used in the determination of the velocity needed for the Reynolds number.

$$U = \sqrt{u_{ax}^2 + u_{lat}^2} \tag{16}$$

An upstream spacer grid can impart a swirl effect inside of a subchannel. This grid-induced swirl will not be captured in the current version of CTF. Currently, lateral velocities are only dependent on mass transfer through the gaps. If there is

swirl, however, the local lateral velocity inside of the subchannel will be larger just after the grid and then decay downstream of the grid as the lateral component weakens due to viscous friction. A factor is used to calculate the additional 'swirl velocity' term that will be added to the current lateral velocity in order to determine the effective lateral velocity in the subchannel. This velocity is then used in the Reynolds number calculation. Figure 3 shows generic profiles with arbitrary units that may result from analysis of the CFD simulations. These profiles show potential relationships between the inlet velocity (x-axis) and the lateral velocity at a certain location downstream of the grid (y-axis). These profiles are captured by capturing the lateral velocity at the location of the rod's surface from a certain axial location in the CFD results.

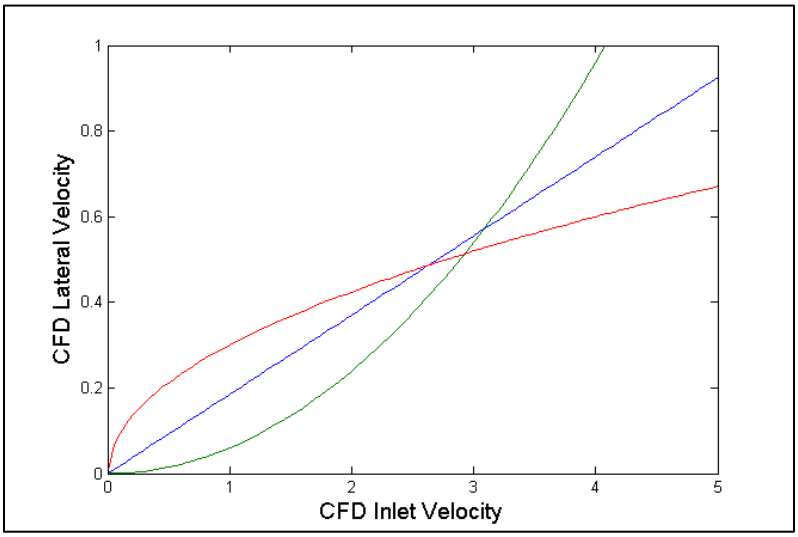

Figure 3: Possible profiles for CFD lateral velocity at the rod surface vs CFD swirl velocity

Figure 3 is shown to illustrate the fact that the correlation between axial velocity and the lateral velocity of the swirl is unknown until the CFD simulations determine this effect. If the CFD simulated lateral velocity, u_{lat}^{CFD}, is found to correlate linearly (shown as the blue line in Figure 3) with the CFD inlet velocity, u_{ax}^{CFD}, then a ratio can be drawn between the two terms:

$$f_{swirl} = \frac{u_{lat}^{CFD}}{u_{ax}^{CFD}} \tag{17}$$

Similarly, the CFD simulations could show that the lateral velocity term is proportional to the square (green line) or square root (red line) of the axial velocity. Then the swirl factor would reflect this and Equation (17) could become:

$$f_{swirl} = \frac{u_{lat}^{CFD}}{(u_{ax}^{CFD})^2} \text{ or } f_{swirl} = \frac{u_{lat}^{CFD}}{\sqrt{u_{ax}^{CFD}}} \tag{18}$$

Since the lateral velocity will diminish due to the viscous forces acting against its motion downstream of the grid, this needs to be appended to the f_{swirl} term to add downstream distance dependence. The decay of the swirl magnitude is expected to be exponential. Then a factor that can capture the intra-channel swirl can be applied to the lateral velocities. It will be something similar to that shown in Equation (19).

$$f_{swirl} = f_{swirl} \exp\left(b\frac{x}{D}\right) \tag{19}$$

Here, b is a coefficient that will specify the length-scale of the decay. x/D is the normalized downstream distance dependent on the hydraulic diameter of the subchannel. When the factor is greater than unity, then it will results in an increase of the calculated Reynolds number and therefore the calculated HTC.

The CFD simulations required to determine these swirl parameters must be performed with a single subchannel in order to capture only the effect of the grid swirl and no crossflow terms from other subchannels. In this manner, the simulated lateral velocity caused by the grid, u_{lat}^{CFD}, is effectively the swirl velocity, u_{swirl}.

$$u_{lat}^{CFD} = u_{swirl} \tag{20}$$

To make this factor applicable to the CTF calculation of the Reynolds number's velocity, the swirl factor should be multiplied by the CTF axial velocity in order to obtain the CTF swirl velocity.

$$u_{swirl} = f_{swirl} u_{ax}^{CTF} \tag{21}$$

Depending on the actual profile of the simulated lateral velocities, Equation (17) or Equation (18) can be used to define an additional term to correct the velocity in the subchannel. This factor should be applied to the lateral velocity terms in the calculation of the Reynolds number used in the HTC correlations. It is not applied to the lateral mass flux value across the gaps, as this can be accounted for in the directed crossflow model. This swirl velocity can then be added to the CTF lateral velocity in order to augment the term with the additional velocity of the swirl caused by the vane.

$$u_{lat}^{CTF} = \left|u_{lat}^{CTF}\right| + \left|u_{swirl}\right| \tag{22}$$

The axial velocity could be modified in the same manner if it is found to be measurably altered by the presence of the grids. The intent of this factor is to only account for the increased velocity across the rod surfaces and therefore the increased heat transfer caused by a larger HTC value. Actually altering the axial and lateral velocities would be a difficult endeavor as CTF only stores a single axial velocity per subchannel per axial level and the lateral velocities are stored by gap. The mass fluxes are calculated in the axial and lateral directions for each subchannel and could be used to determine the velocities using local densities and flow areas. If a factor is simply applied to the local Reynolds number then it will affect the calculation of the HTC while not affecting the flow rates into or out of the fluid cell. This is important for mass/momentum/energy conservation, and is required as the swirl effect needs to be captured on a smaller scale than CTF is capable of modeling—there are no parameters currently in the code other than the entire fluid volume's lateral and axial velocity/flow rate.

$$Re = \frac{\rho U D}{\mu} = \frac{\rho D \sqrt{u_{ax}^{CTF} + \left(\left|u_{lat}^{CTF}\right| + \left|u_{swirl}\right|\right)^2}}{\mu} \tag{23}$$

As mentioned, Equation (23) could be modified to include an additional swirl enhancement term applied to the axial velocity if it is determined that the axial velocity slows an appreciable amount and the effect should be modelled. The main cause of the increased heat transfer is the increase in the lateral velocity, which means more heat can be convected from the rod surface in the same amount of time. The main cause of the lateral velocity is grid's vane angle. A single 'vorticity factor' cannot be used to account for the downstream heat transfer effects as the egg-crate spacers do not cause any real increase in the intra-channel swirl yet they still have a measurable impact on the HTC. Also, this factor would assume that all rod surfaces experience the same increase in lateral velocity. This is not the case for grids which cause a meandering crossflow, as there will be increased velocity on two of the subchannel's rod surfaces but the other two will experience reduced lateral flow—almost a stagnation point in the horizontal dimensions. CTF reports the temperature at each of the rod's four surfaces in its results. There are differences in temperatures around the perimeter of the rod due to the properties of the fluid subchannel in which it is contact. To account for the minimal lateral flow on a portion of the rod surfaces we would need to specify some sort of map across which the meandering flow is applied. This could be done but the user would need to provide more details about the geometry of the grid in order for CTF to capture the effects properly. The effects are expected to decay exponentially downstream of the grid.

Similarly, the Nusselt number ratio (such as is used by the YHL correlation) should not be used for these proposed improvements. We are trying to utilize CFD velocity measurements whenever possible due to their proven reliability and inherent use as modifiers in a subchannel code.

The effects of spacer grids on downstream heat transfer were analyzed by R. Salko [8]. The geometry of the experiment being analyzed contained simple spacer grids as well as mixing vane grids. The downstream HTC values were calculated using the Dittus-Boelter correlation and compared with VIPRE-I (a subchannel code) simulated results with no grid

effects. This produced a ratio of gridded to bare HTC values which are shown in Figure 4 for the MVG and Figure 5 for the SSG.

In Figure 4 the ratio shows that downstream of the MVG, the calculated ratio drops by approximately 40% between the span of the MVGs. This ratio is the experimental HTC to that simulated by VIPRE without using any correction for the grid effects on heat transfer. This can largely be attributed to the motion of the fluid caused by the geometry of the grid vanes. Figure 5 shows the ratio for the SSG. The effect is not as pronounced as that for the MVG but it still shows a decline of approximately 15% which cannot be entirely attributed to lateral velocities due to the fact that simple spacers are not designed to cause swirl or lateral effects. In additions, there is much less variation in the SSG results than in the MVG results.

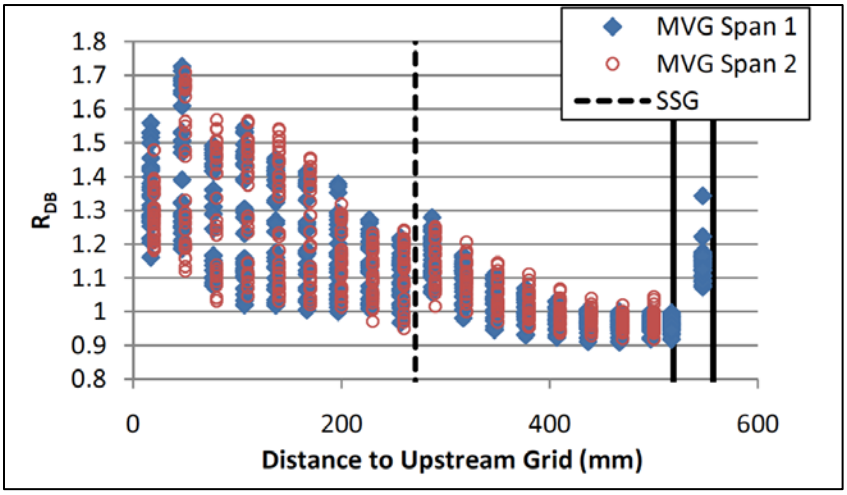

Figure 4: Ratio of MVG experimental HTC to VIPRE-simulated HTC (without grid effects) vs downstream distance [8]

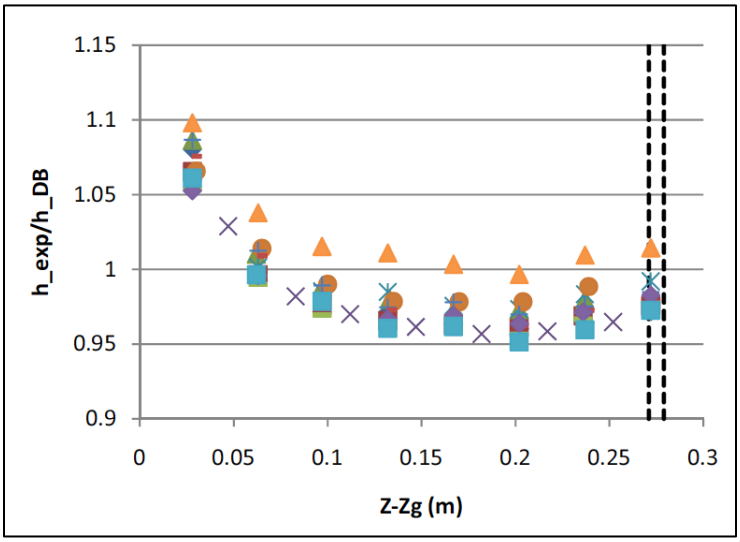

Figure 5: Ratio of SSG experimental HTC to VIPRE-simulated HTC (without grid effects) vs downstream distance [8]

These results imply that there are multiple mechanisms driving the downstream heat transfer effects; it is not simply a function of the vane-driven lateral velocity. Accounting for these other effects with CFD simulations requires quantifying these other mechanisms and accurately predicting them.

In order to obtain the data for the three types of grids, each grid type should be modeled in CFD under certain conditions. The egg-crate grid needs to have its axial velocities measured within the grid's flow area and then apply a factor similar to that found in Equation (19) to the axial velocity used in calculating the Reynolds number, similar to that found in Equation (23). The crossflow mixing vane grid simulations need to capture the detailed tangential velocities along the surface of the rod and then average them to determine an HTC for that corner of the rod surface and its temperature and heat transfer calculations.

Proposed CFD-Informed Grid-Form-Loss Model

Accounting for exact grid geometry instead of relying on the current pressure drop models in CTF gives users an advantage if they have access to the spacer grid designs used in their model. Using CFD measurements of the fluid pressures at axial locations and as a function of vane angle will give data specific to a grid design that can be used within CTF. The idea is to develop a more grid-specific form loss coefficient that can be used in the momentum equation.

Currently, the user can either specify a per-subchannel grid loss coefficient to CTF or else allow CTF to calculate the local grid-loss coefficient based on general grid geometric parameters (e.g. blockage ratio and vane angle). The grid loss coefficient is then used to calculate the $\vec{M}_k^d$ term of Equation (1). For this work, it is proposed that this local grid-loss coefficient be supplied to CTF via an external input file that was generated based on a CFD simulation of that specific grid's geometry. This would leverage the existing CTF ability to take local grid-loss coefficients via input and, therefore, would not require any modification of the CTF governing equations or source code.

The loss coefficient of a grid is generally the sum of the form and friction loss coefficients acting on the grid and its mixing vanes. In the current version of CTF, the local pressure losses (in the vertical direction) caused by the grids are modeled as velocity head losses using:

$$\Delta P = \frac{1}{2}\zeta_{grid}\rho u^2 \tag{24}$$

This form loss is applied to each of the phases and includes ζ_{grid}, the form loss coefficient, u, the vertical fluid velocity, and ρ, the fluid density. The value for ζ_{grid} in Equation (24) can either be supplied by the user at each grid's axial location or can be calculated by the code. The user may specify a different value for each subchannel at a given axial node, offering the opportunity to account for differences in subchannel geometries. If calculated within CTF, it is performed using:

$$\zeta_{grid} = \min\{20, 196\mathrm{Re}_{mix}^{-0.333}\} f_{loss}\left(A_{block}^{spacer} + A_{block}^{springs}\right)^2 \tag{25}$$

If Equation (25) is utilized, the user must supply values for f_{loss}, the pressure loss coefficient multiplier, as well as for the blockage ratios for both the spacer and its springs. Since these are user-supplied values, there is room for improvement using CFD data in this calculation.

The CFD simulations would be utilized to determine form loss coefficients specific to a modelled grid. The pressure drop can be extracted from CFD data at the locations before and after the grid. This should be a surface-averaged value across the entire subchannel. The CFD model can be a single subchannel with the grid in place and four rod surfaces. There should be multiple geometries run in order to cover the different types of subchannels attached to a certain grid. Then, in order to account for the friction pressure drop due to the presence of immobile rod surfaces there needs to be a CFD simulation of a bare subchannel where the pressure drop is measured over the same axial length as was done in the grid's model. Once the rod friction is subtracted to obtain the pressure loss due to the spacer grid, Equation (24) can be utilized to calculate a form loss coefficient as needed.

Summary and Comments on the Proposed Models

The goal of this proposal is to define a path to replace some currently-used thermal-hydraulic correlations in CTF with CFD-supported information where applicable. Most of these correlations are based on data that is not quite relevant to the conditions of an LWR but they are being applied nonetheless. These proposed models could be implemented in the same way as the previously-developed models, which would require an external file with the CFD data. Additionally, hard-coded values for a generic grid design could be added directly to the source for fast modeling of general mixing vane grids. Both options could be used in order to give users the ability to select data from open-source grid data and to be able to provide their own grid data if they are for proprietary calculations. Also, the current external files contain only one numerical value (such as the lateral convection factor) per axial node, per vane angle. If a larger, more accurate simulation is desired, then full geometry models could be utilized to provide multiple values per axial node which would correspond to specific gaps or subchannels in order to account for different subchannel connection geometries.

The challenge of this proposal is to effectively produce and utilize data from CFD simulations in a format that can be used in CTF. The theory and assumptions behind the proposed work rely on the fact that lateral velocities, for example, can be explicitly extracted at discrete axial levels from the CFD simulations and manipulated in a way that is appropriate for use in the CTF source code. Surface- and volume-averaging techniques must be used to produce these sorts of data from the CFD results. The user needs to be able to supply proprietary grid data as necessary and there needs to be a single file required by CTF which will account for the previously discussed spacer grid enhancement factors. This will likely involve breaking the data file into several sections—one for the gap data, one for the velocity data, and one for the loss coefficients.

Path Forward

Once the proper CTF modifications are designated, models are designed, and tests are decided, work will likely begin using STAR-CCM+ as the CFD code. It is well-supported by CD-adapco and has a large user-base. Hydra-TH is the VERA CFD code and can be included in subsequent calculations once preliminary results are derived. While still a powerful single-phase code, Hydra-TH is not quite as beginner-friendly at this point. The methods that are being developed as part of this work will be applicable to any type of CFD code and no direct coupling will be required. Multiplicative factors can be regenerated using any type of CFD code once the CTF infrastructure for taking the data is in place.

References

[1] M. Avramova, “Development of an Innovative Spacer Grid Model utilizing Computational Fluid Dynamics within a Subchannel Analysis Tool”, PhD Thesis, The Pennsylvania State University, 2007.

[2] R. Salko, M. Avramova, “CTF Theory Manual”, The Pennsylvania State University, 2014.

[3] M. Avramova, “CTF/STAR-CD Off-Line Coupling for Simulation of Cross-flow Caused by Mixing Vane Spacers in Rod Bundles”, Proceedings: International Conference on Mathematics and Computational Methods Applied to Nuclear Science and Engineering (M&C 2011), Rio de Janeiro, Brazil, May 8-12, 2011.

[4] A. Lewis, R. Smith, B. Williams, “An Information Theoretic Approach to Use High-Fidelity Codes to Calibrate Low-Fidelity Codes”, CASL-U-2014-0197-000, 2014.

[5] T. Chun and D. Oh, “A Pressure Drop Model for Spacer Grids with and without Flow Mixing Vanes”, Journal of Nuclear Science and Technology, Vol. 35, pgs. 508-510, 1998.

[6] R. Salko, et al., “CTF – A Thermal-Hydraulic Subchannel Code for LWRs Transient Analyses: Users’ Manual”, The Pennsylvania State University, 2014.

[7] S. Yao, L. Hochreiter, W. Leech, “Heat-Transfer Augmentation in Rod Bundles Near Grid Spacers”, Journal of Heat Transfer, Vol. 104, pgs. 76-81, 1982.

[8] R. Salko, “Data Analysis and Modeling of NESTOR SSG Heated Rod Bundle Experiment using VIPRE-I for the Assessment of the Onset of Nucleate Boiling Criterion”, M.S. Thesis, The Pennsylvania State University, 2010.

Appendix A

This appendix contains the CFD cross-flow external data file required for CTF simulations where the user specifies the grid-directed cross-flow option. The first line of numbers is the dimensions of the table (axial values, number of vane angles) and then the data are grouped in columns by vane angle. The left-most column contains the axial values [m] and the top-most row contains the vane angles [°]. The rows correspond to the axial locations along the model. The values shown have been abridged. Use of the grid-directed cross-flow model requires this input file as well as the input file shown in Appendix B.

```
****************************************************
* 2D table for lateral flow rate
****************************************************
           260             4             0             0
*
  1
*
         10.     20.     30.     40.
0.00  0.0000  0.0000  0.0000  0.0000
0.23  0.0001  0.0001  0.0001  0.0001
0.24  0.0001  0.0001  0.0001  0.0001
0.25  0.0001  0.0001  0.0001  0.0001
0.26  0.0001  0.0001  0.0001  0.0001
0.27  0.0002  0.0002  0.0002  0.0002
0.28  0.0002  0.0002  0.0002  0.0002
0.29  0.0001  0.0001  0.0001  0.0001
0.30  0.0001  0.0001  0.0001  0.0001
...
...
2.98  0.0238  0.0509  0.0596  0.0638
2.99  0.0238  0.0509  0.0596  0.0638
3.00  0.0238  0.0509  0.0596  0.0638
```

Appendix B

This appendix contains the mapping data that the user must supply in an external file for the grid-directed cross-flow modeling option in CTF. These are the gap numbers in the first column and the sign of the direction in the second column. If the value is zero, then no cross-flow is assumed across that gap. Positive values correspond to flow from the lower-numbered subchannel to the higher-numbered subchannel connected to the gap. These data are represented visually in Figure 1.

```
  1   0.0
  2   0.0
  3   0.0
  4   0.0
  5   0.0
  6   0.0
  7   0.0
  8   0.0
  9   0.0
 10   0.0
 11   0.0
 12   0.0
 13   0.0
 14  -1.0
 15   1.0
 16   1.0
 17  -1.0
 18  -1.0
 19   1.0
 20   0.0
 21  -1.0
 22   0.0
 23   0.0
 24   0.0
 25   1.0
 26   1.0
 27  -1.0
 28   1.0
 29  -1.0
 30  -1.0
 31   0.0
 32   1.0
 33   0.0
 34   0.0
 35   0.0
 36  -1.0
 37  -1.0
 38  -1.0
 39   1.0
 40   1.0
 41  -1.0
 42   0.0
 43  -1.0
 44   0.0
 45   0.0
 46   0.0
 47  -1.0
 48   0.0
 49   1.0
 50   0.0
 51  -1.0
 52   0.0
 53   0.0
 54   0.0
 55   0.0
```

```
56   0.0
57   0.0
58   0.0
59   0.0
60   0.0
```

Appendix C

This appendix contains the CFD data required for the enhanced turbulent mixing option in CTF. The first line of numbers specifies the number of axial values and the number of vane angles for which data are provided. The table is then grouped in columns by vane angle and in rows by axial location. The left-most column contains the axial values [m] and the top-most row contains the vane angles [°]. This table is abridged.

```
****************************************************
* 2D table for the spacer multiplier
****************************************************
           105             2             0             0
*
  1
*
           0.0    15.0
0.0000  1.0000  1.0032
0.7524  1.0000  1.0032
0.7824  1.0000  1.1260
0.8124  1.0000  4.0587
0.8424  1.0000  2.7668
0.8724  1.0000  1.7056
0.9024  1.0000  1.1480
0.9324  1.0000  0.9104
...
...
3.9744  1.0000  1.1480
4.0044  1.0000  0.9104
4.0100  1.0000  0.8245
```